

## Characteristics of Flow over a Double Backward-Facing Step

S. Wang<sup>1</sup>, D. Burton<sup>1</sup>, J. Sheridan<sup>1</sup> and M. C. Thompson<sup>1</sup>

<sup>1</sup>Fluids Laboratory for Aeronautical and Industrial Research (FLAIR)  
Department of Mechanical and Aerospace Engineering  
P.O. Box 31, Monash University, Clayton, 3800, Australia

### Abstract

A *double backward-facing step* (DBFS) is a sequence of two steps with the distance between the steps in the fluid flow direction representing a variable parameter. For this research, the flow characteristics of a DBFS are studied numerically as a function of this distance, with each step height equal and constant. The flow is characterised in terms of the reattachment lengths of the recirculation bubbles behind each step, the overall flow topology and the base pressure on the vertical step surfaces. The predictions are based on two-dimensional (2D) Computational Fluid Dynamics (CFD) simulations using Reynolds-Averaged Navier-Stokes (RANS) turbulence models.

### Introduction and Literature Review

The flow over a *single backward-facing step* (SBFS) is a classic problem in fluid dynamics and has been extensively studied. Although it is one of the simplest geometries, it exhibits rich flow physics, including flow separation, flow reattachment, and multiple recirculating bubbles [12].

In 1983, Armaly et al. [2] conducted a systematic study of a SBFS and reported additional regions of flow separation downstream of the step and on both sides of the channel test section, which is not documented in previous studies [10]. Therefore, that study is regarded as a milestone in this area, and much subsequent research has been conducted while referencing that paper. The reattachment length of the recirculation bubble is an important feature, and its behaviour over a range of Reynolds number, step surface roughness, expansion ratio and width-to-height ratio conditions has been studied [3, 9, 12].

A *double backward-facing step* (DBFS) is a sequence of two steps with the distance between the steps in the fluid flow direction representing a variable parameter. In contrast to the SBFS, the DBFS has received little attention from fluid mechanists. A variant of DBFS flow is that associated with a ship-like object of finite span, placed in an open-air environment, where the first step is between the upper and lower deck, and the second step between the lower deck and the water surface. Based on particle image velocimetry (PIV) and qualitative oil-flow visualisations, Tinney and Ukeiley [11] proposed that the flow over a ship-like 3D DBFS object consists of a combination of flow elements, including a horseshoe vortex, horizontal entrainment of air and the presence of two counter-rotating vortices initiated at reattachment. Herry et al. [4] further investigated the stability of this flow and found that the mean flow field can be described by at least two solutions at zero-degree drift angle, with those two solutions mutually symmetric.

In recent years, researchers have started to focus attention onto the DBFS, as it has some practical significance to the automotive and marine industries. For the marine industry, understanding the typical flow field structure around the flight deck, which is normally simplified to a DBFS geometry, has important significance in analysing the interaction between the helicopter

rotors and the airwake behind the ship [8]. For the automotive industry, a utility vehicle, also known as a pickup truck, can be approximated as a DBFS over its rear half. Understanding the near-wake flow of a utility vehicle provides valuable information on drag reduction and consequent fuel savings [1].

Based on these and other potential practical applications, it is apparent that understanding the flow over a DBFS has some practical significance. Even though the flow behaviour of a ship airwake and flow over a pickup truck have both been studied, an understanding of the underlying fundamental flow physics is still very limited. Here, we undertake a systematic study to investigate the fundamental flow physics of DBFS flow. Important flow features are quantified including the reattachment length, formation of recirculation bubbles and base pressure variations of the step surfaces.

### Numerical Method

#### Preliminary Simulations

In this study, we focus on the flow over a two-dimensional DBFS. To provide confidence in the CFD simulations for the DBFS, two SBFS flow problems are studied. These phases of the research are referred as stages 1 and 2. In the first stage, the experimental set-up of Armaly et al. [2] is reproduced. The CFD simulations investigate the influence of turbulence model, mesh resolution and blockage. As determined by Armaly et al. [2], the bulk flow structure is primarily two dimensional when the flow is fully turbulent for  $Re > 6000$ . These 2D simulations are conducted in this fully turbulent flow regime. We compared reattachment length and time-mean flow structure predictions for the  $k-\epsilon$  (both the standard and enhanced wall treatment model), SST  $k-\omega$ , standard  $k-\omega$  and Spalart-Allmaras (S-A) turbulence models. The results show that SST  $k-\omega$  turbulence model is the most appropriate turbulence model, providing the best fit to the experimental data on reattachment length as the Reynolds number is varied. This concurs with observations of Menter [6] for similar flow conditions.

An orthogonal block-structured grid is used for this stage to provide better grid point placement control at boundaries and within the domain. Based on grid independence tests, the flow field effectively converges to within 0.23% when each step face consists of 60 to 80 divisions. As this study is based on a high expansion ratio flow (outlet to inlet height ratio equals 1.36), to validate the CFD settings for an open case, for which the top boundary is removed, a second validation stage is carried out. The CFD settings obtained from the stage 1 are then applied to predict the reattachment length results of Kostas et al. [5], which has low expansion ratio of 1.02. Based on the consistency of the experimental and numerical results, it is concluded that the CFD settings (i.e., resolution, turbulence model, etc.) are also valid for this case. Thus, based on these two validation cases, the preferred solver settings and meshing strategy are applied to the subsequent DBFS flow simulations.

**Project Description**

The flow over a DBFS is studied using 2D steady-state RANS simulations. The Reynolds number is 20,000, calculated based on the freestream velocity and the combined heights of the two steps. The flow is in the turbulent regime, so it is not anticipated that the flow behaviour will be highly sensitive to Reynolds number.

The domain of the CFD simulation is illustrated in figure 1 below. Each step has a height of  $h$ . The distances in front of the first step and behind the second step are  $50h$  and  $75h$  respectively, and the heights of the inlet and outlet are  $50h$  and  $52h$  respectively. This gives an expansion ratio of  $52/50 = 1.04$ . The distance between the steps is characterised by the variable,  $d$ . The domain has 4 boundaries, and the corresponding boundary conditions for the inlet, outlet, upper boundary and ground (including step faces) are velocity inlet, pressure outlet, symmetry, and no-slip wall. The turbulent intensity level at inlet and outlet is 1%, and the corresponding turbulent length scale is 10% of the step height ( $h$ ). Cases of  $d/h$  between 0 and 10, with an increment of 1 are studied.

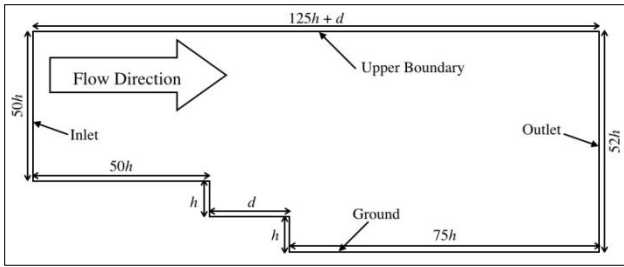


Figure 1: Layout of the computational domain (not to scale).

The solver used in this project is ANSYS FLUENT, 64-bit commercial software, and the simulations are discretised by finite-volume method based on the RANS approach. The turbulence model chosen is SST  $k-\omega$ . A pressure-based, implicit coupled solver, based on second-order upwind discretisation is used to converge the initial guess to provide an accurate steady-state (time-mean) solution. Convergence is assumed when the residuals of continuity, momentum, turbulent kinetic energy and specific dissipation rate equations reach a level of  $10^{-6}$  or better.

**Grid Description and Refinement**

An orthogonal block-structured grid with higher resolution over the recirculation regions is the general meshing strategy, with inflation layers applied at all wall boundaries to capture the boundary layers. The adequacy of the near-wall inflation layers is checked by monitoring the converged values of the turbulence-wall Y-plus parameter. In order to fully solve the boundary layer to determine the position of reattachment and separation, the values of Y-plus near the steps are kept near 1. An enhanced wall treatment is used, which allows the solution close to the walls to be computed explicitly.

A finer grid is applied to the region where the flow behaviour is expected to be more complex, such as the recirculation regions. In order to avoid the loss of discretisation accuracy due to a sudden change in the lengths of adjacent cells, the expansion ratio between any two adjacent cells is kept below 1.1.

Additionally, a mesh convergence study based on the geometry for  $d/h=10$  is applied to investigate grid independence. The meshing strategy for each grid is identical, while the number of cells is gradually increased from 0.03 to 2.2 million. The mesh convergence test is based on the primary reattachment length behind the first step, and the results are plotted in figure 2. The results indicate that the mesh achieves grid independence when the number of cells is 1.3 million. This gives 80 divisions for

each step base and 50 divisions per step height. This grid density is applied for all other cases.

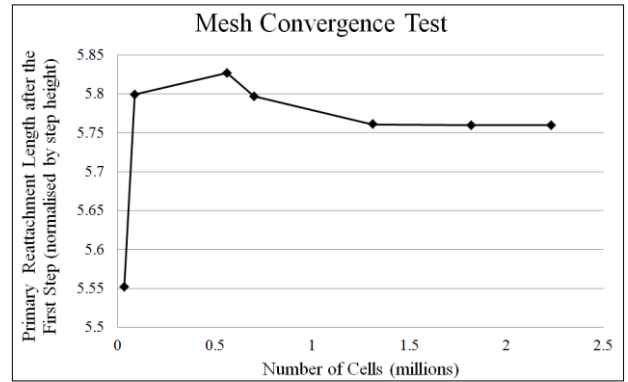


Figure 2: Mesh convergence study.

**Result Analysis**

The results in this study are presented from two perspectives: overall result analysis and individual case analysis. In the first section, the variations of reattachment length and step base pressure coefficient with  $d/h$  from 0 to 10 are presented and analysed. In the second section, more detailed flow field results for distinctive individual cases (i.e.  $d/h = 0, 1, 3, 5$  and  $6$ ) are presented. Note that all lengths, e.g., the reattachment length, are normalised by the step height ( $h$ ). The step base pressure coefficient is calculated based on the freestream velocity and the reference pressure at the outlet (i.e., 0 units). The reattachment length is determined based on the extrapolation of the zero-velocity line along the wall [2]. The intensity of the vortex is quantified by the magnitude of the stream function, which describes the mass flow rate of recirculating fluid within each individual recirculation bubble.

**Overall Result Analysis**

**1. Reattachment Length Variation with  $d/h$**

As  $d/h$  varies from 0 to 10, the flow structure can be divided into two regimes, as shown in figure 3. The top sketch shows the typical flow behaviour for  $d/h$  between 1 and 5, with the flow separating at the first step and reattaching downstream of the second step. For cases of  $d/h$  from 6 to 10, the recirculation bubbles downstream of the first and second step become independent, as shown in the bottom sketch in figure 3. When  $d/h$  equals 0, the geometry reverts to a SBFS with the step height of  $2h$ . The reattachment length for each recirculation bubble is defined in figure 3, where the  $d_0$  represents the overall reattachment length of the entire DBFS.

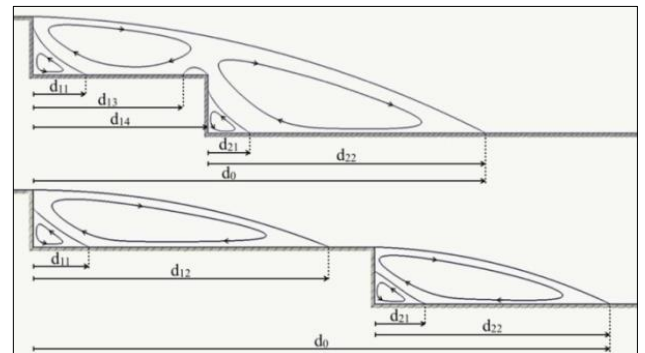


Figure 3: Schematic highlighting the recirculation bubbles and respective reattachment lengths.

The change in the reattachment lengths as  $d/h$  is varied between 0 and 10 is illustrated in figure 4. In the first regime, as the second step is shifted away from the first step, a small recirculation

bubble is formed at  $d_{13}$  when  $d/h$  is 3 and then disappears when  $d/h$  is greater than 4. In the second regime, as the second step is shifted further downstream, the sizes of the recirculation bubbles behind the two steps become near identical as the differences between  $d_{11}$  and  $d_{21}$ , and  $d_{12}$  and  $d_{22}$  are reduced. Additionally, the overall reattachment length ( $d_0$ ) does not increase until the second step is six step heights from the first.

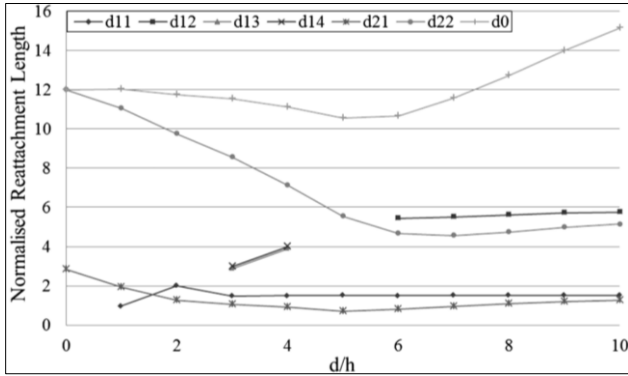


Figure 4: Variation of the reattachment lengths as  $d/h$  is varied between 0 and 10.

## 2. Step Base Pressure Coefficient Variation with $d/h$

The base pressure coefficient is calculated based on the average surface pressure at each step base, and its variation with  $d/h$  is plotted in figure 5. For  $d/h = 0$ , the first and second step coincide. Thus the average  $C_p$  of the two step bases are identical for  $d/h = 0$ . When the second step is shifted downstream, the difference of the average  $C_p$  between the two steps gradually increases, and achieves the maximum at  $d/h = 6$ . With the second step shifted even further downstream, the difference of step base pressure coefficient between the two steps reduces.

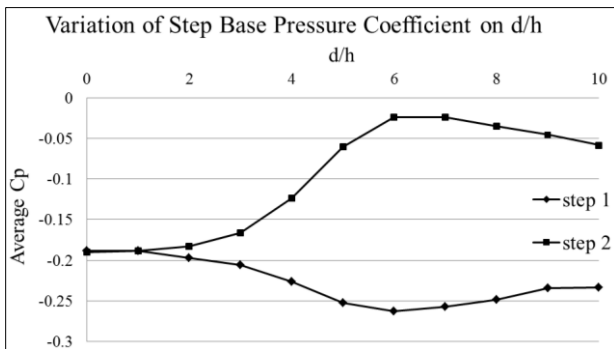


Figure 5: Variation of the step base pressure coefficient as  $d/h$  is varied between 0 and 10.

## Individual Case Analysis

### Case 1: $d/h = 0$

At  $d/h = 0$ , the double backward-facing step is equivalent to a SBFS with a step height of  $2h$ . This is used as a reference case to calculate the vortex intensity. To compare the relative strength of the different recirculation bubbles, the *intensity* of a vortex is represented by the magnitude of stream function difference between the recirculation centre and dividing outer streamline, normalised by the value for vortex A (the primary recirculation bubble of  $d/h = 0$ ). The flow structure is presented by the streamlines as shown in figure 6, and the intensities of vortices are presented in Table 1. The flow structure is identical to the flow structure for a SBFS. This consists of a primary recirculation bubble (i.e., vortex A) and a corner vortex (i.e., vortex B). Due to the high grid resolution in this study, a tiny tertiary eddy is captured at the step corner (this feature also exists

occasionally in other cases). This series of vortices is in line with the theory of *Moffatt eddies* in a concave corner [7]. Because the size of this eddy is extremely small and its influence on the main flow structure is negligible, information about this eddy is not reported in the present study.

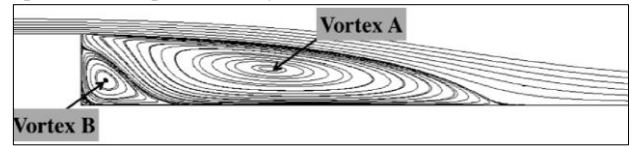


Figure 6: Streamlines showing the recirculation bubbles behind the step ( $d/h = 0$ ).

	Intensity of Vortices (normalised)
$d/h$	0
Vortex A	1
Vortex B	0.061

Table 1: Intensity of vortices ( $d/h = 0$ )

### Case 2: $d/h = 1$

The flow structures for  $d/h = 1$  and 2 are very similar, consequently only the  $d/h = 1$  case is presented here. When the second step is shifted away from the first step, a corner vortex is formed behind each step (vortices D and E), as shown in figure 7. The corner vortices at  $d/h = 1$  and 2 are weaker than the corner vortex in the single step case (i.e.,  $d/h = 0$ ). The intensity of each vortex is presented in table 2.

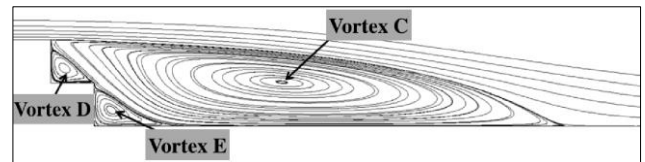


Figure 7: Streamlines showing the recirculation bubbles behind the steps ( $d/h = 1$ ).

	Intensity of Vortices (normalised)	
$d/h$	1	2
Vortex C	1.013	0.962
Vortex D	0.034	0.027
Vortex E	0.017	0.032

Table 2: Intensity of vortices ( $d/h = 1$  and 2)

### Case 3: $d/h = 3$

In this case the primary recirculation bubble, as shown in the previous cases, breaks into two vortices (vortices F and G). Due to the similarity of the flow structure of  $d/h = 3$  and 4, only the flow structure for  $d/h = 3$  is presented in figure 8. Additionally, as the second step is shifted from  $d/h = 3$  to 4, the intensity of vortex F remains almost identical, while the intensity of vortex G drops significantly, as shown by the results in table 3. At this stage, apart from the major recirculation bubbles (i.e., vortices F and G) and corner eddies (i.e., vortices H and I), a tiny recirculation bubble (vortex J) is formed at above the edge of the second step, associated with separation of reversed flow.

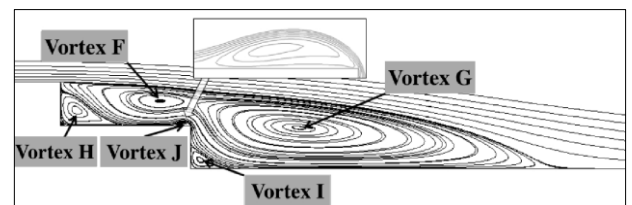


Figure 8: Streamlines showing the recirculation bubbles behind the steps ( $d/h = 3$ ).

$d/h$	Intensity of Vortices (normalised)	
	3	4
Vortex F	0.441	0.460
Vortex G	0.873	0.647
Vortex H	0.029	0.030
Vortex I	0.022	0.018
Vortex J	0.010	0.004

Table 3: Intensity of vortices ( $d/h = 3$  and  $4$ ).

#### Case 4: $d/h = 5$

When the second step is five step heights from the first step, the small recirculation bubble above the edge of the second step disappears, as illustrated in figure 9. This is the last case before the recirculation bubbles behind the two steps effectively become independent. Additionally, the intensity of the primary recirculation bubble behind the first step (i.e., vortex K) surpasses the intensity of the primary recirculation bubble behind the second step (i.e., vortex L), as presented in table 4.

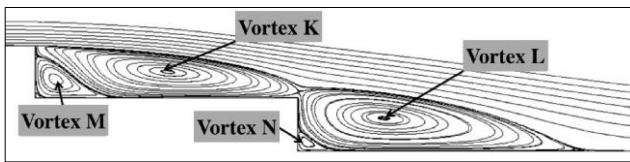


Figure 9: Streamlines showing the recirculation bubbles behind the steps ( $d/h = 5$ ).

$d/h$	Intensity of Vortices (normalised)	
	5	
Vortex K	0.461	
Vortex L	0.351	
Vortex M	0.033	
Vortex N	0.010	

Table 4: Intensity of vortices ( $d/h = 5$ )

#### Case 5: $d/h = 6$

When the distance between the two steps is increased to six step heights, the main recirculation zones behind each step become fully separated, as illustrated in figure 10. From  $d/h = 6$  on, the flow firstly reattaches behind the first step. Moving further downstream, the boundary layer further develops until it reaches the edge of the second step, and then the flow reattaches behind the second step. Additionally, as the second step is shifted further downstream, the difference between the vortices behind the first and second step reduces (see table 5), as the influence of the upstream vortices (vortices O and Q) on downstream flow field is reduced.

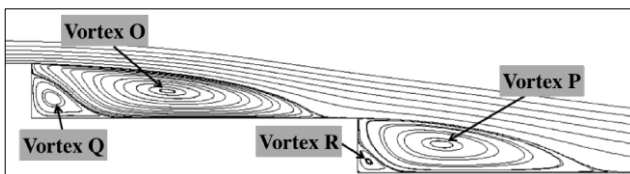


Figure 10: Streamlines showing the recirculation bubbles behind the steps ( $d/h = 6$ ).

$d/h$	Intensity of Vortices (normalised)				
	6	7	8	9	10
Vortex O	0.462	0.461	0.461	0.449	0.459
Vortex P	0.262	0.276	0.305	0.317	0.345
Vortex Q	0.033	0.033	0.033	0.031	0.032
Vortex R	0.011	0.017	0.022	0.024	0.027

Table 5: Intensity of vortices ( $d/h = 6, 7, 8, 9$  and  $10$ )

## Conclusions

In conclusion, the characteristics of the time-mean DBFS flow with different configurations (i.e.,  $d/h$  varying between 0 and 10) were investigated by solving for the flow field based on the 2D Reynolds-Averaged Navier–Stokes equations. A number of distinct flow regimes were identified. The flow behaviour had been quantified based on the variation of reattachment lengths, intensities of the associated vortices and step base pressure.

## Acknowledgements

This research was supported under Australian Research Council's Linkage Projects funding scheme, project number LP130100953, and computing time support from the National Computational Infrastructure (NCI) (project d71) are gratefully acknowledged.

## References

- [1] Al-Garni, A.M. and L.P. Bernal, *Experimental study of a pickup truck near wake*. J. Wind Eng. Ind. Aerodyn., 2010. **98**(2): p. 100-112.
- [2] Armaly, B.F., et al., *Experimental and theoretical investigation of backward-facing step flow*. J. Fluid Mech., 1983. **127**: p. 473-496.
- [3] Biswas, G., M. Breuer, and F. Durst, *Backward-facing step flows for various expansion ratios at low and moderate Reynolds numbers*. J. Fluids Eng.-Trans. ASME, 2004. **126**(3): p. 362-374.
- [4] Herry, B.B., et al., *Flow Bistability Downstream of Three-Dimensional Double Backward Facing Steps at Zero-Degree Sideslip*. J. Fluids Eng.-Trans. ASME, 2011. **133**(5).
- [5] Kostas, J., J. Soria, and M.S. Chong, *Particle image velocimetry measurements of a backward-facing step flow*. Experiments in Fluids, 2002. **33**(6): p. 838-853.
- [6] Menter, F.R., *Two-equation eddy-viscosity turbulence models for engineering applications*. AIAA journal, 1994. **32**(8): p. 1598-1605.
- [7] Moffatt, H.K., *Viscous and resistive eddies near a sharp corner*. Journal of Fluid Mechanics, 1964. **18**(01): p. 1-18.
- [8] Reddy, K.R., R. Toffoletto, and K.R.W. Jones, *Numerical simulation of ship airwake*. Comput. Fluids, 2000. **29**(4): p. 451-465.
- [9] Schafer, F., M. Breuer, and F. Durst, *The dynamics of the transitional flow over a backward-facing step*. J. Fluid Mech., 2009. **623**: p. 85-119.
- [10] Taylor, T. and E. Ndefo. *Computation of viscous flow in a channel by the method of splitting*. in *Proceedings of the Second International Conference on Numerical Methods in Fluid Dynamics*. 1971. Springer.
- [11] Tinney, C.E. and L.S. Ukeiley, *A study of a 3-D double backward-facing step*. Exp. Fluids, 2009. **47**(3): p. 427-438.
- [12] Wu, Y., H. Ren, and H. Tang, *Turbulent flow over a rough backward-facing step*. International Journal of Heat and Fluid Flow, 2013.